Analysis of Triangular Rollable and Collapsible Composite Booms under the Effects of Gravity and Twist

Richard A. Larson[1[0000-0001-8525-3557]], Cyrus J. R. Kosztowny[2[0000-0003-4603-6861]], William Allen Waters, Jr.[1] and David Long[1]

[1] Analytical Mechanics Associates, Hampton, VA 23666
[2] NASA Langley Research Center, Hampton, VA 23681

Abstract. Finite element analysis is used to investigate Triangular Rollable and Collapsible (TRAC) composite booms. The TRAC booms are subjected to a suite of loading conditions, including in-plane bending, out-of-plane bending, and axial compression. Simulations containing as-designed boom geometry are performed, as are simulations with geometric deviations associated with the as-built conditions of a sample TRAC boom. Namely, a cross-sectional twist along the length of the boom is incorporated into the analysis to study the effect of the twist on the deformation characteristics of the boom. Twisting in the sample boom was observed after short-term storage in a rolled configuration and may be attributed to differential creep deformation between the inner and outer flanges of the TRAC boom. Simulations are conducted with and without the effects of gravity to understand the significance of gravity on testing conditions. Booms of three lengths are evaluated: 3 meters, 7.5 meters and 30 meters. The mechanical responses of the TRAC booms are discussed with reference to the effects of gravity, boom length and cross-sectional twisting. Gravity is found to have a more significant effect on boom mechanical response as boom length is increased. Cross-sectional twisting is found to have a more significant effect on boom mechanical response in the shorter booms.

Keywords: High Strain Composites, Deployable Structures, Finite Element Analysis.

1 Introduction

High-strain composites have proven to be useful for deployable composite structures since they can be packed into a smaller state without being damaged [1]. The stowed state of a high-strain composite deployable structure is useful as the structure will occupy less volume when launched into space and can be deployed as a larger structure once in orbit. In particular, the deployable structure of interest herein is a boom, a relatively long and rigid spar that is used to support payloads, scientific instruments, or other deployable technologies such as solar sails [2].

At NASA Langley Research Center, high-strain composite deployable booms are being investigated to assess their performance under microgravity conditions under the Gravity Offloading and Analysis of Long Imperfection-Sensitive Elements (GOALIE) project. Several types of composite booms currently exist for space applications and are illustrated in Fig. 1. The first use of a deployable boom occurred in 1961 with the design by Klein of the Storable Tubular Extendible Member (STEM) for an antenna on Canada's first satellite, the Alouette. The STEM was a slit tube cross section boom, as shown in Fig. 1, this boom would roll up flat and as it deployed the cross section would again become circular and part of the main structure. Lenticular booms [3] (Fig. 1) consist of two axially symmetric omega shaped shells and are also well understood and have been used on the recently launched Advanced Composite Solar Sail System (ACS3) mission [4]. One final boom cross section of note is the Triangular, Rollable and Collapsible (TRAC) boom cross section. The TRAC boom was developed by the Air Force [5, 6] and a metal version of the TRAC boom has been used on three solar sail missions – NanoSail-D [7], LightSail-1 [8] and LightSail-2 [9].

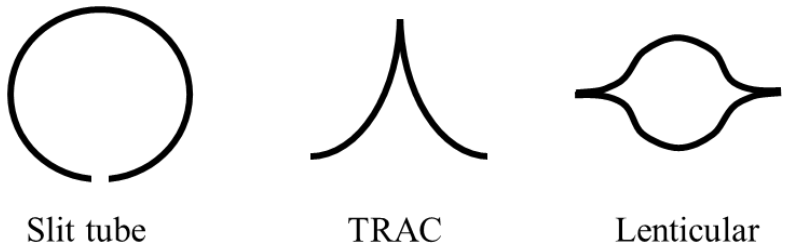

Fig. 1. Different historically used deployable boom cross sections.

In the present study, composite TRAC booms are investigated as they have been identified as a possible enabling technology for large solar sails such as the 1,672 m^2 sail used on the Solar Cruiser project [10]. Metal TRAC booms are very sensitive to temperature gradients while in space due to their relatively high coefficient of thermal expansion as compared to their composite counterpart. While in orbit, one side of the boom may be in direct sunlight and the opposing side is enveloped in shadow. The combination of the asymmetric cross-section and resulting temperature gradients through the boom's cross-section can yield significant out-of-sail-plane deflections on the order of 0.5 m for a 4 m long boom [11]. Also, TRAC booms offer a high second moment area along a single plane of symmetry. For solar sail application, TRAC booms can offer high resistance to out-of-sail plane bending when oriented along the plane of symmetry of the TRAC boom's cross-section.

Experimentally evaluating high-aspect ratio (very long and slender) booms is challenging. While these booms are designed for use with spacecraft that operate in microgravity, the effects of gravity are present in tests conducted on the Earth. Thus, if hanging a long boom with the cross-section oriented horizontally, the boom will sag and buckle under its own weight unless supported properly via a system such as a wiffle tree. Other challenges in testing and characterizing long boom behavior come from linking multiple sub-systems into one global data acquisition system, as well as facility

size and space required to house a structure of 30 m length (as studied herein) or longer. To ease some of these challenges, the planned testing of this 30 m boom will take place with the boom hung vertically and as such the boom will herein be simulated in an "as hung", vertical condition.

In this paper the influence of several factors on composite TRAC boom mechanical behavior is investigated. Factors of interest include gravity, boom length and boom as manufactured condition. Three boom lengths are considered: 3 m, 7.5 m and 30 m. Each boom is subjected to idealized loading conditions, including in-plane bending, out-of-plane bending, and axial compression. First, finite element analysis (FEA) methods are described, including general description of boundary conditions, implementation of cross-sectional twist to represent the as manufactured state, load introduction for each load case and a summary of all analyses performed. Next, the results of the analyses are presented and discussed. Finally, conclusions about how boom length, gravity and inclusion of twist affect the boom response are presented and planned validation methods are discussed.

2 Computational approach

The cross-sectional dimensions of the analyzed boom are presented in Fig. 2. Fabrication of the TRAC boom involves a secondary bonding process. First, two arc shaped half-sections are cured before the second process of bonding the two together at the plane of symmetry for the TRAC boom cross section. Thus, there is a bond line at the plane of symmetry for the cross section. Analysis is performed for booms that are of 3 m, 7.5 m, and 30 m in length. For all three lengths, analysis is performed with and without the effects of gravity. In the cases of the 7.5 m and 30 m booms, cross-sectional twisting along the boom axis is also analyzed. The twisted boom simulations are only performed under the presence of gravity, as the twist incorporated mimicked twisting observed in test articles that will be tested in the presence of gravity.

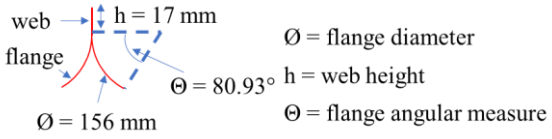

Fig. 2. TRAC boom nominal cross-sectional details.

Abaqus/Standard[1] [12] is used to perform non-linear simulations of boom structural response. Reduced integration shell elements (S4R) are used to model the boom and the load introduction tab at the boom distal end. The two flanges and the web are modeled as separate parts. A tie constraint is used to join the flanges to the web, and to join

[1] The use of trademarks or names of manufacturers in this report is for accurate reporting and does not constitute an official endorsement, either expressed or implied, of such products or manufacturers by the National Aeronautics and Space Administration.

the web to the load introduction tab. Contact is enforced between the inside surfaces of each flange (Fig. 3). The general element size is 10 mm x 5 mm. The 3 m models have 13,779 elements and 14715 nodes. The 7.5 m models have 34,412 elements and 36,665 nodes. The 30 m models have 137,671 elements and 146,515 nodes.

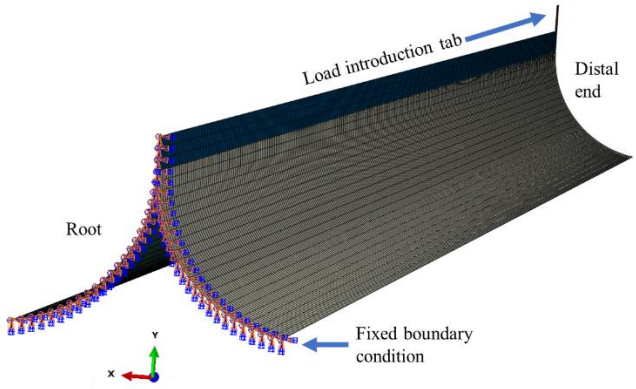

Fig. 3. Meshed 3 m boom and boundary conditions, view from root.

In each simulation, the nodes on the root-most cross section have all degrees of freedom constrained (Fig. 3). The applied displacement boundary conditions for all simulations are shown in Fig. 4. At the distal end, the end-most node of the load introduction tab has an applied displacement in a singular direction. The magnitude of displacement applied varies by load case and boom length but is significant for observation of structural collapse and decreased load carrying capability. Two load steps are performed during the analysis. In the first step, the force of Earth's gravity is applied to the whole model. In the second step, an applied displacement is applied to the distal end.

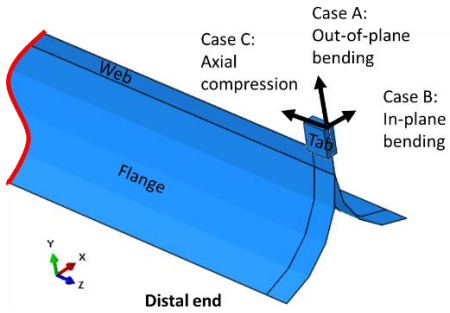

Fig. 4. Distal end details and three fundamental load cases.

As shown in Fig. 4, load case A is the out-of-plane bending load case, load case B is the in-plane bending load case, and load case C is the axial compression load case. The end-most node of the tab is not constrained to only move in the direction of interest, for

example, while moving in axial compression, the distal end is still free to move out of plane. By keeping the loading conditions as simple as possible, the fundamental response of the boom can be observed.

The layup of each flange is $[45_{PW}, 0_{UD}, 90_{UD}, 0_{UD}, 45_{PW}]_s$, where the PW subscript signifies a plain-weave ply and UD signifies a unidirectional ply. Both UD and PW plies have 36% PMT-F7 resin content, the PW plies have MR70 fibers, whereas the UD plies have M40J fibers. For the simulation, the flanges and web are modeled using composite sections in Abaqus, where the web layup contains plies from both flanges and a layer of adhesive. The adhesive used was PMTF7_1A. Each plain weave ply is modeled as 10 separate plies of the layup $[\pm 45°]_{5s}$ where each ply is assigned one tenth of the thickness of the true woven ±45° ply thickness [13]. The material properties used in the Abaqus simulation are tabulated in Table 1, where the PW properties are those for each of the individual 1/10 ply thickness representations as is the reported PW thickness.

Table 1. Material properties

	PW	UD	Adhesive	Aluminum
E1 (Pa)	1.80E+11	2.11E+11	3.50E+09	7.17E+10
E2 (Pa)	7.38E+09	7.45E+09	-	-
E3 (Pa)	7.38E+09	7.45E+09	-	-
nu12	0.284	0.283	0.37	0.33
nu13	0.284	0.283	-	-
nu23	0.444	0.442	-	-
G12 (Pa)	3.57E+09	3.62E+09	-	-
G13 (Pa)	3.57E+09	3.62E+09	-	-
G23 (Pa)	2.55E+09	2.58E+09	-	-
Thickness (m)	4.20E-06	5.59E-05	1.02E-04	0.01
Density (kg/m^3)	1.56E+03	1.54E+03	1246	2810

Upon unspooling and hanging of the 7.5 m TRAC boom test article, it was noted that the cross-section of the boom at the distal end was rotated about the boom axis by approximately 45° with respect to the cross section at the root. The influence of this twisting on the structural response is of interest and as such, this twisting is incorporated into the 7.5 m and 30 m boom models. As this analysis effort is intended to inform upcoming testing and the 3 m boom is not intended to be a test article, nor was assignificant twisting observed in the 3 m boom, twisting is not incorporated into the 3 m boom model. Likewise, the influence of this twisting is only investigated in models that also contain the effects of gravity.

Twist is incorporated adjusting the initial boom geometry. The entire cross section is rotated about the point at which the flanges join the web. The twist level is incorporated linearly from the root to the distal end, with 0° of twist at the root and 45° at the distal end. For the twisted simulations, the load introduction tab is changed from shell elements to a group of beam elements (B31) with one end tied to the center of the web distal end cross section. This change is done to avoid twisting the load introduction tab to mate to the web top surface. In some cases of extreme convergence difficulty, the beam elements used for load introduction are also left out, and the load is applied directly to the node at the top corner of the web at the distal end.

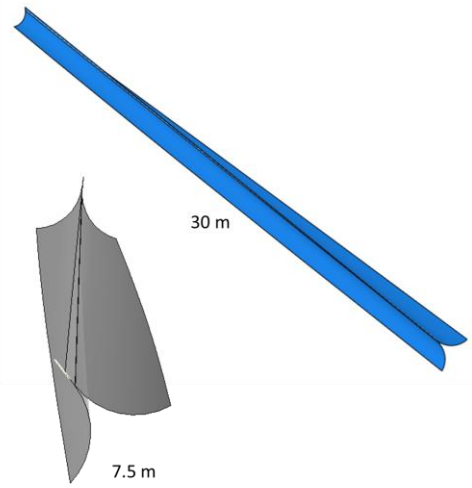

Fig. 5. Twisted booms.

In addition to modification of the load introduction member, one additional modification to the modeling approach is made to achieve convergence. This modification is shown in Fig. 6, and involves altering how the flanges are attached to the web. In the first approach, as described at the beginning of this section, each flange is modeled separately from the web and a tie constraint is used to join the top of each flange to the bottom of the web. In the alternate approach, the flange is modeled with inclusion of the portion of the web, and then the two web halves are tied together. The modifications made to each model to achieve convergence, if any, are noted in the model summary table (Table 2) in section 4.

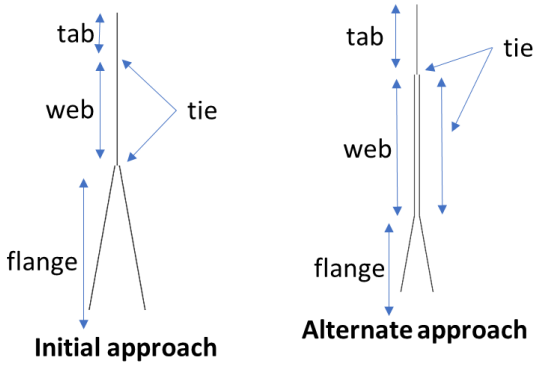

Fig. 6. Alternate tie approach.

Results for the different analyses performed are discussed in section 3 and summarized in section 4. In short, each of three lengths of boom, (3 m, 7.5 m and 30 m) is evaluated for three load cases, with and without inclusion of the effects of gravity. For the two lengths that will be used for upcoming testing (7.5 m and 30 m), additional analysis with 45° boom twist is performed under the effects of gravity for each of the three load cases.

3 Results

3.1 3 meter boom

Inclusion of gravity in the 3 m boom analyses has differing effects depending on how the boom is loaded (Fig. 7). For load case A (Fig. 7a), inclusion of gravitational effects results in a significant decrease in peak load carrying capability. Without gravity, the boom reaches a peak load of 46.57 N, whereas the boom reaches a peak load of 22.36 N with gravity. For load case B (Fig. 7b), no noticeable effect was observed by the inclusion of gravity and the peak load of 10.2 N is observed. For load case C (Fig. 7c), inclusion of gravity results in a mild increase (approximately 14%) in peak load. Without gravity, the boom reaches a peak load of 342.37 N, whereas the boom reaches a peak load of 404.97 N with gravitational effects included. The collapse event is not significantly changed by inclusion of gravity. For load case A, the boom collapses in the web near the root. For load case B, the boom twists until the boom can globally displace and a collapse occurs in the flange near the root. For load case C, the boom fails by flattening at the distal end.

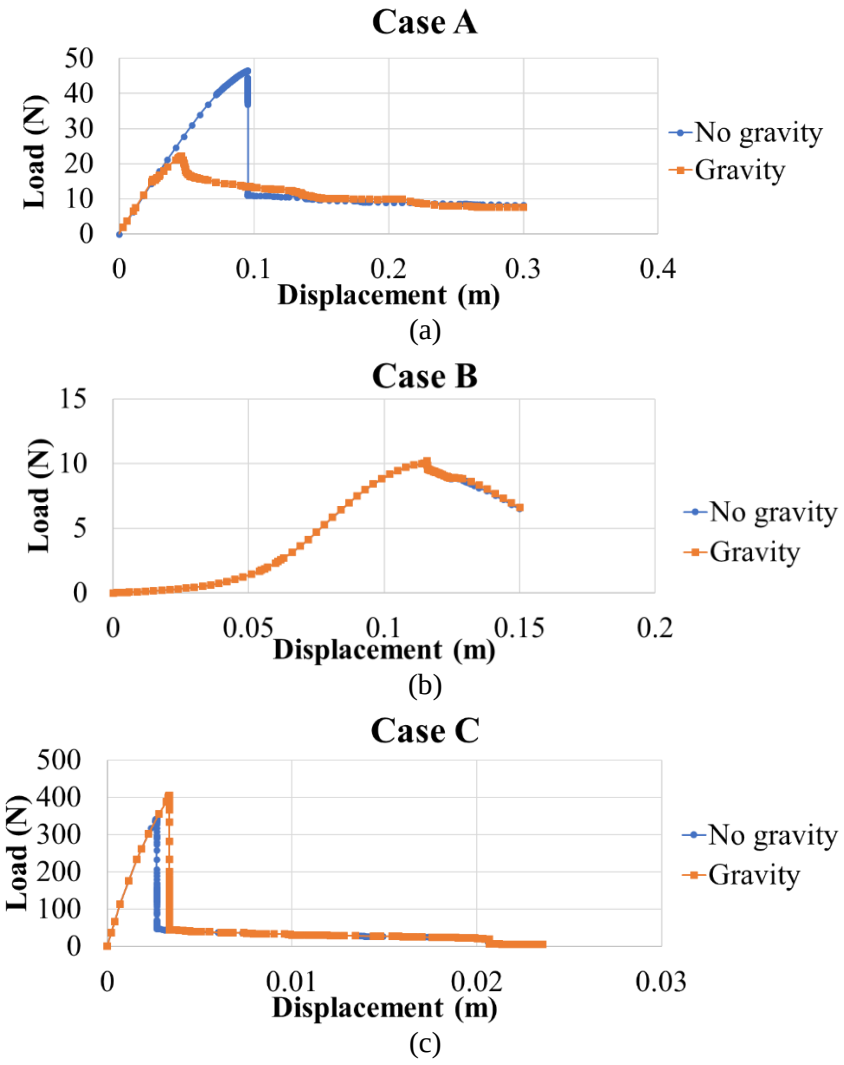

Fig. 7. Load vs. displacement of 3 m boom.

3.2 7.5 meter boom

For the 7.5 m boom, incorporation of twist results in a decreased peak load and a reduction in the load-displacement slope (stiffness) relative to the gravity case for all load cases (Fig. 8), although this effect is least impactful for load case B. Inclusion of gravity has minor effects on the peak load and stiffness in load cases B and C. For load case A (Fig. 8a), however, including gravity results in a slight increase in peak load from 12.26 N to 13.75 N. Incorporation of twist results in a decrease in peak load from 13.75 N to 8.88 N for load case A and a decrease in peak load from 168.99 N to 79.05 N for load case C (Fig. 8c).

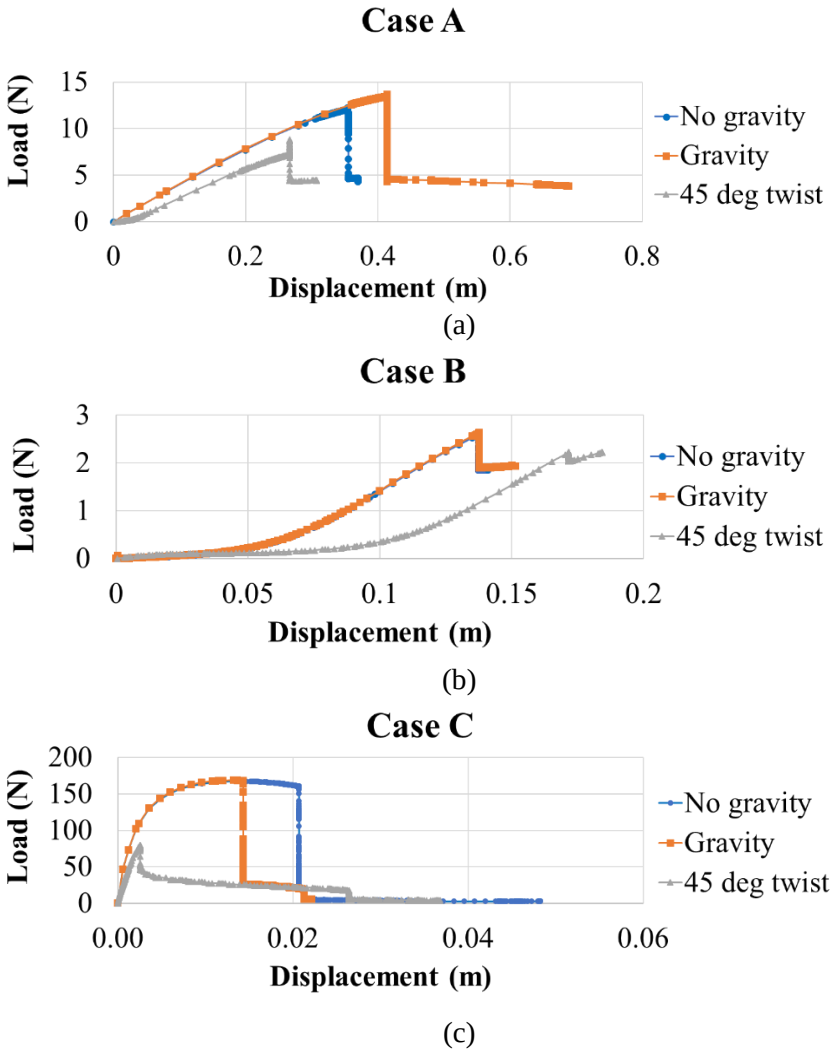

Fig. 8. Load vs. displacement of 7.5 m booms.

Generally, as displacement is applied for load case B (Fig. 8b), the cross section at the distal end of the boom twists until the boom reaches a stable state and the whole boom begins to bend. When the boom is pre-twisted, additional displacement is required to return the boom to an untwisted state as shown in Fig. 9. Once the boom begins bending as a structure, a linearly stiff response is observed in the load vs. displacement of the boom (Fig. 9). This stiffness of the pre-twisted boom is similar to the un-twisted version once the structure is in bending, the difference in displacement level required to bring the structure into bending is a result of the additional displacement required to return the boom to the straight state (Fig. 9).

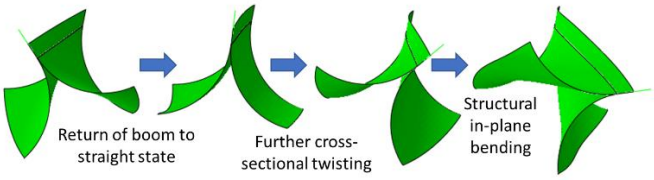

Fig. 9. Twisted 7.5 m boom response to in-plane bending load (load case B).

Boom collapse is predicted by the 7.5 m analysis under load case C, and the tip of the boom flattens. Afterward, the flattened region migrates up the boom towards the root from the tip (Fig. 10). The booms without twist are more resistant to the tip flattening than the twisted case, which fails at a much lower displacement level. Still, the failure response of the cases with and without gravity are quite similar to the response of the case with twist pictured in Fig. 10.

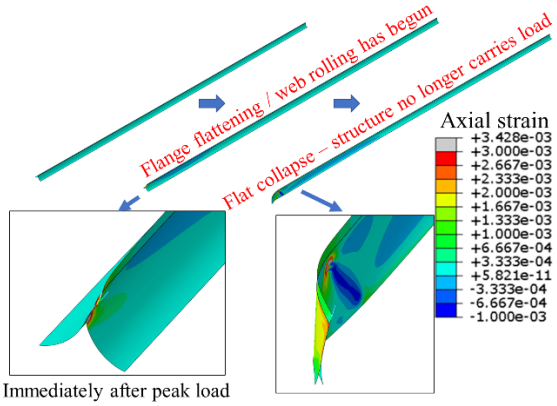

Fig. 10. Deformation characteristics of 7.5 m boom subjected to axial compression (load case C).

3.3 30 meter boom

The load-displacement response for the 30 m boom subjected to all load cases and loading conditions (No gravity, gravity, and 45° twist) is shown in Fig. 11. For the 30 m boom analysis case A (Fig. 11a), incorporation of twist results in decreased peak load relative to the gravity case. Inclusion of gravity in all cases results in increased peak load and stiffness for the 30 m boom. A similar effect for the 30 m boom load case B is observed as for the 7.5 m boom (Fig. 11b), wherein the pre-twisted boom buckles at a higher applied displacement but retains a similar stiffness and peak load as the gravity-only case. Incorporation of twist results in a decrease in peak load from 3.99 N to 3.26 N for load case A and a decrease in peak load from 22.89 to 22.85 N for load case C (Fig. 11c). For load case B, incorporation of twist results in a small increase in peak

load, from 0.75 N to 0.79 N. Between the different load cases, the peak load varies significantly, spanning three different orders of magnitude for the three cases.

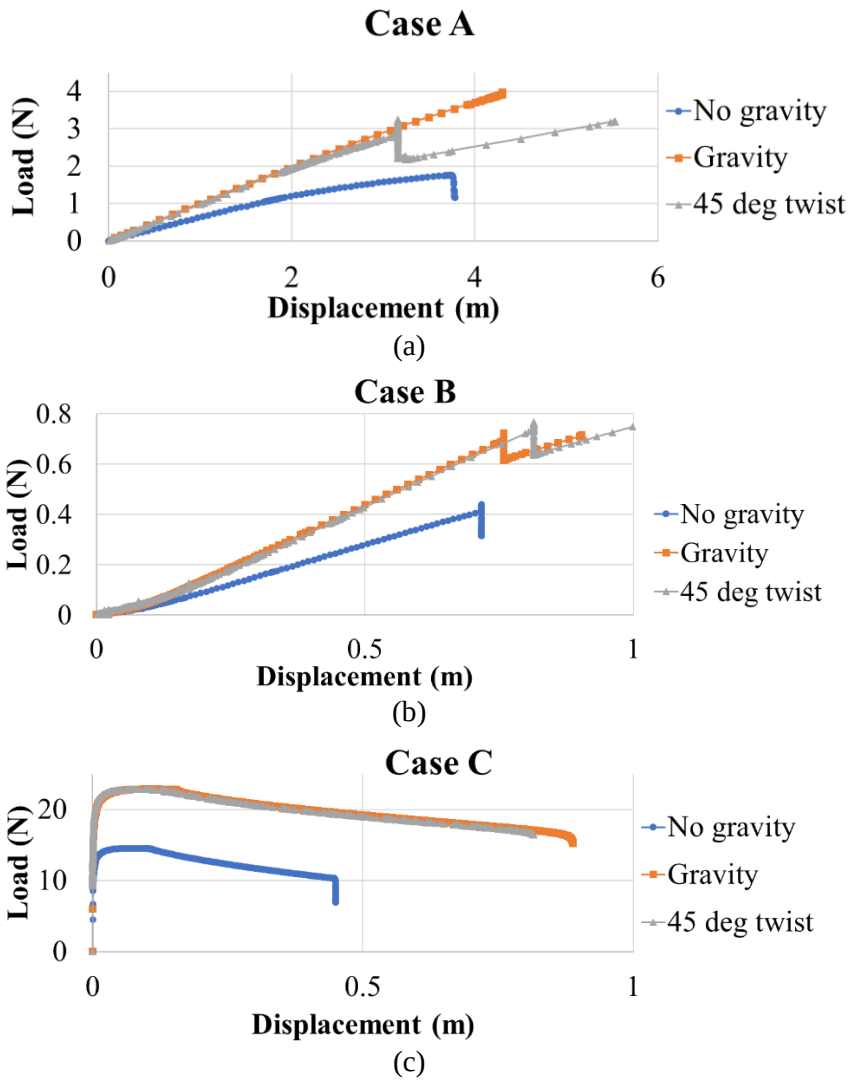

Fig. 11. Load vs. displacement of 30 m booms.

For case A, the boom with gravity has a similar failure mechanism to that without gravity, despite the differences in stiffness and strength. While in twisted form, load case A fails a bit further away from the root, but that is the only major difference in failure mode between the three simulations (Fig. 12). For case A, local web buckling develops near the root that is only slightly visible in the first strain image for each

analysis in both the twisted and without gravity cases. The local buckling becomes more significant as the boom is loaded further until ultimately structural collapse occurs near the root.

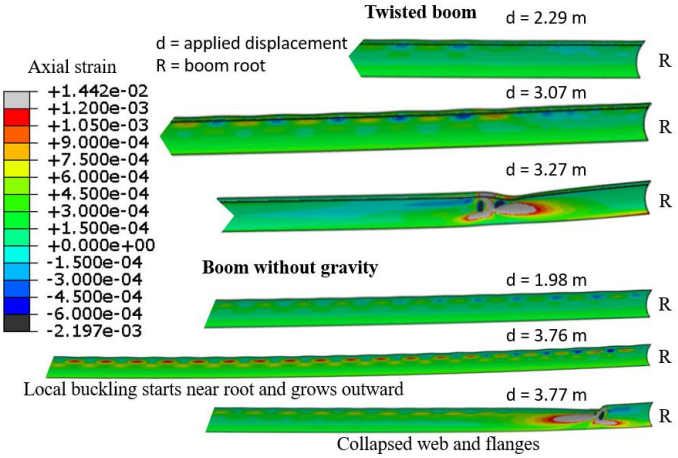

Fig. 12. Deformation characteristics for a 30 m boom subjected to out-of-plane bending (load case A).

For load case B, there are no significant differences observed in the failure mode between the no-gravity and pre-twisted loading conditions, as illustrated in Fig. 13. For load case B, a strain concentration grows close to the root and an additional strain concentration slightly further from the root is observed. Ultimately, the flange buckles by "pinching" in the "valley" between the two strain concentrations Fig. 13.

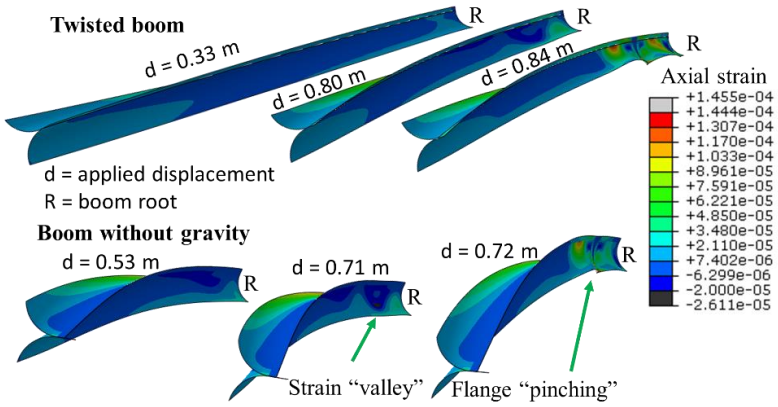

Fig. 13. Deformation characteristics of 30 m boom subjected to in-plane bending (load case B).

For load case C, for the case without gravity at failure, much of the boom reaches very high strain levels and simultaneously a slight buckle develops in the web near the root. These high strain levels are indicative that global buckling would occur at the root wherein strain energy would be released either by the boom folding on itself or breaking, but the current simulation fidelity is indicative of catastrophic failure at this region. The case with incorporated twist bends significantly closer to the center of the boom, until ultimately the entire structure collapses at this location, similarly to the simulation with gravity and no twist (Fig. 14).

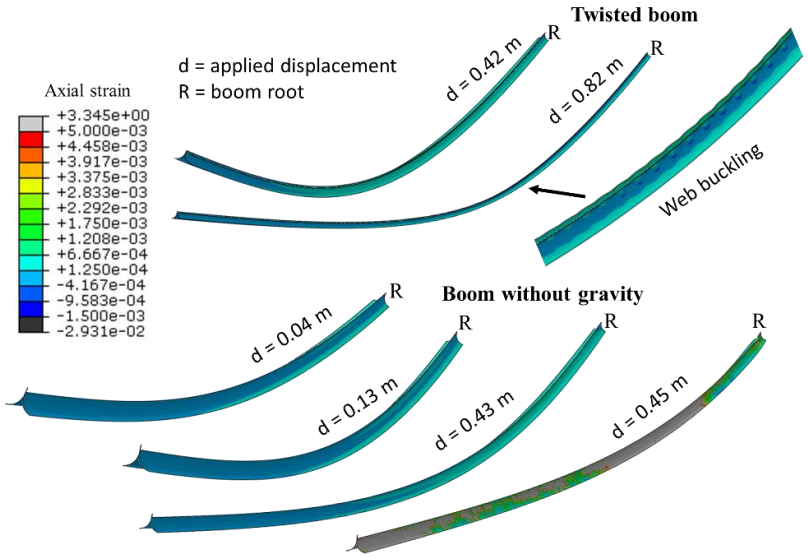

Fig. 14. Deformation characteristics of a 30 m boom subjected to axial compression (load case C).

4 Discussion

4.1 Effects of gravity, length, and pre-twist

A summary of the peak load, deflection from wing root, and observed buckling location for all load cases and pre-conditions (gravity and pre-twist) is provided in Table 2. Discussion of these results is presented in detail in this section. One interesting point to note is that the 45° of twist is significantly greater twist per meter for the 7.5 m boom as compared with the 30 m boom.

Table 2. Analysis summary

Boom length	Load case	Gravity	Twist	Convergence modifications	Peak load (N)	Distance of failure to root (m)	Buckled member
3	A	no	no	none	46.57	0.46	web
3	B	no	no	none	10.15	1.51	flange
3	C	no	no	none	342.37	3	all
3	A	yes	no	none	22.36	0.15	web
3	B	yes	no	none	10.2	1.52	flange
3	C	yes	no	none	404.97	3	all
7.5	A	no	no	none	12.26	2.1 and 0.49	web
7.5	B	no	no	none	2.59	1.82	flange
7.5	C	no	no	none	167.15	7.5	all
7.5	A	yes	no	none	13.75	2.07	web
7.5	B	yes	no	none	2.64	1.83	flange
7.5	C	yes	no	none	168.99	7.5	all
7.5	A	yes	yes	none	8.88	0.43	web
7.5	B	yes	yes	none	2.22	0.174	flange
7.5	C	yes	yes	none	79.05	7.5	all
30	A	no	no	alternate tie constraint used	1.77	0.39	web
30	B	no	no	alternate tie constraint used	0.43	2.75	flange
30	C	no	no	none	14.57	0.34	web/all
30	A	yes	no	none	3.99	0.44 and 6.79	web
30	B	yes	no	none	0.75	2.43	flange
30	C	yes	no	none	22.89	12.4	all
30	A	yes	yes	Load applied direct to web	3.26	0.73	web
30	B	yes	yes	Load applied direct to web	0.79	3 and 0.27	flange
30	C	yes	yes	Load applied direct to web	22.85	12.7	all
Load case A = out of plane bending, case B = in plane bending, case C = axial compression							

The effect of gravity has differing influence on the booms depending on boom length and load case. For load case B, gravity has the least significant effect on boom behavior. Gravity has a greater effect for the 30 m booms and results in increased stiffness and strength. Whereas for the 3 m and 7.5 m booms, gravity does not change the structural stiffness and the effect of gravity on the strength follows no clear trend.

As boom length increases, the largest effect is a decrease in peak loads in all cases. This decrease in strength is because the longer booms can buckle more easily as compared to the shorter booms. This behavior is consistent with classical Euler-Bernouli beam theory of long-slender beams subjected to axial compression. Due to the simple boundary conditions, a difference in buckling behavior is clearly observed in load case C boom response once the boom length reaches 30 m. For the shorter booms the tip of the boom flattens at failure, whereas for the 30 m boom the boom tip significantly moves out-of-plane, resulting in a failure location more similar to load case A. In previously performed analyses [13], if out of plane displacement was restricted, as opposed to the boundary condition with simple displacement in the axial direction, the flattening of the tip would still be the failure mode.

Twisting has little effect on stiffness of the 30 m boom. Twisting results in decreased strength for all cases except in load case B for the 30 m boom, in which strength increases by 0.04 N. The decrease in strength is most significant for load cases A and C on the 7.5 m boom. For load case B, the twist does result in additional displacement at failure, but ultimately, this displacement in the load case B response is simply attributed to the straightening of the boom prior to loading it. This effect in load case B (for all lengths) highlights the very low torsional stiffness expected of a TRAC boom.

5 Conclusions

5.1 Closing remarks

Analysis was performed for three different lengths of TRAC booms and two preconditions (with and without the effects of gravity, and with incorporation of twist). The effects of gravity were demonstrated to become increasingly significant as boom length increases. Also, as boom length increases, peak buckling load was shown to decrease. The significance of gravity on long booms, in addition to lower load carrying capability, highlights the difficulties that will be encountered with experimentally testing TRAC booms and the importance of future gravity-offloading concepts.

Lessons learned about fundamental boom behavior with the simplified boundary conditions herein give good insight into how and where composite TRAC booms can fail under different major load cases. The lessons learned will inform data collection setup for the experimental article. Analysis methods used herein will be modified to closer represent conditions associated with experimental testing. Upcoming experimental work will serve to validate the models developed herein and those developed representative of the experimental test set up.

References

1. Liu, T.-W., Bai, J.-B., Xi, H.-T., Fantuzzi, N., Bu, G.-Y., Shi, Y.: Experimental and numerical investigation on folding stable state of bistable deployable composite boom. Compos. Struct. 320, 117178 (2023)
2. Liu, T.-W., Bai, J.-B., Fantuzzi, N., Zhang, X.: Thin-walled deployable composite structures: A review. Prog. Aerosp. Sci. 146, 100985 (2024)
3. Herbeck, L., Leipold, M., Sickinger, C., Eiden, M., Unckenbold, W.: Development and Test of Deployable Ultra-Lightweight CFRP-Booms for a Solar Sail. In: European Conference on Spacecraft Structures, Materials and Mechanical Testing., Noordwijk, The Netherlands (2000)
4. Wilkie, W.K.: Overview of the NASA Advanced Composite Solar Sail System (ACS3) Technology Demonstration Project. In: AIAA Scitech 2021 Forum. American Institute of Aeronautics and Astronautics, VIRTUAL EVENT (2021)
5. Leclerc, C., Pellegrino, S.: Ultra-Thin Composite Deployable Booms. Proc. IASS Annu. Symp. 2017, 1–9 (2017)
6. Banik, J., Murphey, T.: Performance Validation of the Triangular Rollable and Collapsible Mast. Small Satell. Conf. (2010)
7. Johnson, L., Whorton, M., Heaton, A., Pinson, R., Laue, G., Adams, C.: NanoSail-D: A solar sail demonstration mission. Acta Astronaut. 68, 571–575 (2011)
8. Biddy, C., Svitek, T.: LightSail-1 solar sail design and qualification. In: Proceedings of the 41st Aerospace Mechanisms Symposium. pp. 451–463, Pasadena, CA (2012)
9. Betts, B., Spencer, D., Nye, B., Munakata, R.: Lightsail 2: Controlled solar sailing using a CubeSat. In: The 4th International Symposium on Solar Sailing. , Kyoto, Japan (2017)
10. Johnson, L., Everett, J., McKenzie, D., Tyler, D., Wallace, D., Wilson, J., Newmark, J., Turse, D., Space, R., Cannella, M., Feldman, M., Aerospace, B.: The NASA Solar Cruiser Mission – Solar Sail Propulsion Enabling Heliophysics Missions.
11. Stohlman, O.R., Loper, E.R.: Thermal Deformation of Very Slender Triangular Rollable and Collapsible Booms. Presented at the 2016 AIAA SciTech Conference, San Diego, CA January 4 (2016)
12. Abaqus/Standard User's Manual, Version 2023 (2023)
13. Nguyen, L., Medina, K., McConnel, Z., Lake, M.S.: Solar Cruiser TRAC boom development. In: AIAA SCITECH 2023 Forum. American Institute of Aeronautics and Astronautics (2023)